Chemical Science

EDGE ARTICLE

View Article Online
View Journal | View Issue

Check for updates

Cite this: *Chem. Sci.*, 2023, **14**, 171

All publication charges for this article have been paid for by the Royal Society of Chemistry

High-yield production of liquid fuels in CO_2 hydrogenation on a zeolite-free Fe-based catalyst†

Lisheng Guo, *[a] Xinhua Gao, [b] Weizhe Gao,[c] Hao Wu,[a] Xianbiao Wang,[a] Song Sun, *[a] Yuxue Wei,[a] Yasuharu Kugue,[c] Xiaoyu Guo,[c] Jian Sun *[d] and Noritatsu Tsubaki *[c]

Received 9th September 2022
Accepted 16th November 2022

DOI: 10.1039/d2sc05047a

rsc.li/chemical-science

Catalytic conversion of CO_2 to long-chain hydrocarbons with high activity and selectivity is appealing but hugely challenging. For conventional bifunctional catalysts with zeolite, poor coordination among catalytic activity, CO selectivity and target product selectivity often limit the long-chain hydrocarbon yield. Herein, we constructed a singly cobalt-modified iron-based catalyst achieving 57.8% C_{5+} selectivity at a CO_2 conversion of 50.2%. The C_{5+} yield reaches 26.7%, which is a record-breaking value. Co promotes the reduction and strengthens the interaction between raw CO_2 molecules and iron species. In addition to the carbide mechanism path, the existence of Co_3Fe_7 sites can also provide sufficient O-containing intermediate species (CO*, HCOO*, CO_3^{2}*, and HCO_3^*) for subsequent chain propagation reaction *via* the oxygenate mechanism path. Reinforced cascade reactions between the reverse water gas shift (RWGS) reaction and chain propagation are achieved. The improved catalytic performance indicates that the KZFe–5.0Co catalyst could be an ideal candidate for industrial CO_2 hydrogenation catalysts in the future.

Introduction

With the extensive use of carbon-based fossil fuels, the concentration of CO_2 in the atmosphere has reached a record high, and this rising level creates a series of ecological problems such as ocean acidification and global warming.[1,2] Carbon capture, utilization and storage (CCUS) is regarded as a powerful strategy for reducing the CO_2 concentration.[2–5] Chemical valorization of CO_2 into valuable chemicals or fuels is a promising route to turn waste into treasure and reduce the detrimental effects of greenhouse gas. Long-chain hydrocarbons, as carbon-neutral fuels, have high energy density and facile mobile storage capacity, and have attracted wide attention.[6–9] Owing to the inertia of CO_2 molecules and imprecise control of carbon chain propagation during CO_2 hydrogenation, efficient catalytic conversion of CO_2 into long-chain hydrocarbons remains a huge challenge.[10,11]

Iron-based catalysts can form two kinds of active sites *in situ* (Fe_3O_4 for RWGS, and Fe_xC_y for chain propagation) during reaction, and thus have been widely used in CO_2 hydrogenation.[12] To increase the C_{5+} selectivity or break the Anderson–Schulz–Flory (ASF) distribution, various strategies have been adopted to regulate the activity and product selectivity over iron catalysts. Doping with alkali promoters (K, Na, Mn, *etc.*) is a typical case.[6,13] The existence of alkali promoters is beneficial for improving CO_2 adsorption behaviors and Fe carbonization. Especially in recent years, metal oxides have been combined with zeolite to form bifunctional catalysts that show benign performance for CO_2 hydrogenation. It is worth mentioning that although these novel composite catalysts (*e.g.*, Na–Fe_3O_4/HZSM-5 and In_2O_3/HZSM-5) generally exhibit a high C_{5+} selectivity, their low catalytic activity (10–30%) and high CO by-product (20–60%) selectivity generally limit the effective yield of C_{5+} or lower the catalyst (metal oxide + zeolite) time yield.[7,8]

In addition, the introduction of a second active metal has been adopted.[14,15] The second active metal is generally involved in the reverse water gas shift (RWGS) and/or chain propagation processes.[14,16,17] Currently, the incorporation of a second active metal has been extensively used to improve the CO_2 hydrogenation process.[14–16,18,19] In terms of conventional Fischer–Tropsch synthesis (FTS), Co catalysts present higher chain growth ability than iron catalysts. In contrast, single Co catalysts produce large amounts of CH_4 instead of long-chain products in CO_2 hydrogenation. Interestingly, the introduction of an appropriate amount of Co into Fe-based catalysts can

[a]School of Chemistry and Chemical Engineering, Anhui University, Hefei, Anhui 230601, China. E-mail: lsguo@ahu.edu.cn; suns@ustc.edu.cn
[b]State Key Laboratory of High-Efficiency Utilization of Coal and Green Chemical Engineering, College of Chemistry & Chemical Engineering, Ningxia University, Yinchuan 750021, PR China
[c]Department of Applied Chemistry, School of Engineering, University of Toyama, Gofuku 3190, Toyama 930-8555, Japan. E-mail: tsubaki@eng.u-toyama.ac.jp
[d]Dalian National Laboratory for Clean Energy, Dalian Institute of Chemical Physics, Chinese Academy of Sciences, Dalian 116023, China. E-mail: sunj@dicp.ac.cn

† Electronic supplementary information (ESI) available. See DOI: https://doi.org/10.1039/d2sc05047a

result in unique catalytic behavior. Xu *et al.* synthesized a $ZnCo_xFe_{2-x}O_4$ catalyst for the selective conversion of CO_2 into light olefins (36.1% for $C_{2-4}^{=}$), and ascribed the phenomenon to the optimized generation of iron–cobalt carbide, Co_2C, and h-Fe_3C phases.[15] Similarly, Kim *et al.* suggested that the high olefin selectivity (39.0% for $C_{2-4}^{=}$) is due to the facile formation of a unique bimetallic alloy carbide $(Fe_{1-x}Co_x)_5C_2$.[19] Zhang *et al.* reported that a Na-modified CoFe alloy catalyst using a layered double-hydroxide (LDH) precursor is conducive to the formation of C_8–C_{16} jet-fuel-range hydrocarbons.[14] However, although the C_{5+} selectivity reaches 72.9%, the CO_2 conversion in this case is only 10.2%. Guo *et al.* adopted Co doping to increase conversion activity (60.4%) and reduce CO selectivity (4.5%) with moderately decreased C_{5+} selectivity (20.7%).[16] Based on the above inspiration, we wondered whether the introduction of Co metal would be promising to maintain high activity while maintaining high selectivity of C_{5+} products without the utilization of zeolite. Therefore, it is significant to understand tailor-made Fe catalysts with Co regulation for the efficient conversion of CO_2 to long-chain hydrocarbons with high catalytic activity.

Herein, different from conventional composite catalysts for oriented synthesis of heavy hydrocarbons, we report how iron-based catalysts can be optimized *via* cobalt incorporation to realize efficient catalysts for CO_2 hydrogenation to long-chain hydrocarbons with high-yield production. The Co-modified iron catalyst exhibits a low CO selectivity (8.1%) and a high selectivity toward C_{5+} hydrocarbons (57.8%) at a CO_2 conversion of 50.2%, in which the yield of C_{5+} reaches 26.7%. With the introduction of Co, the cascade reactions between RWGS and chain propagation are notably reinforced, and the product distribution deviates from the ASF model *via* an oxygen-containing intermediate (CO*, HCOO*, CO_3^{2}*, and HCO_3^*) pathway.

Results and discussion

The molar ratio of Co/Fe is summarized in Table S1.† The results are close to the designed value. CO_2 hydrogenation performance tests over different catalysts were conducted, and the results are depicted in Fig. 1a and S1.† The KZFe catalyst exhibits a high C_{5+} selectivity of 49.9% at a CO_2 conversion of 48.3%, and the main products are olefin-rich hydrocarbons.

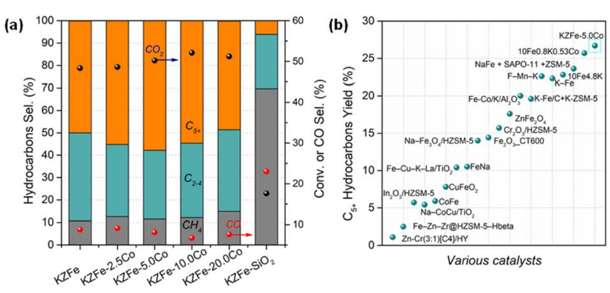

Fig. 1 (a) Catalytic performances of as-prepared catalysts for CO_2 hydrogenation at 320 °C, 2.0 MPa, and 6000 mL g^{-1} h^{-1}. (b) Catalytic yields of C_{5+} hydrocarbons over various catalysts. Yield = CO_2 conv. × (1 − CO sel.) × C_{5+} sel. Catalysts (in (b)) from left to right were cited from ref. 6–8, 14 and 20–32.

Previous studies have also demonstrated that a $ZnFe_2O_4$ catalyst containing K as a promoter is conducive to the formation of heavy olefins.[16] Alkali K promotes the carburization of iron species and enhances chain propagation ability. To further demonstrate this promotional effect derived from the spinel $ZnFe_2O_4$ structure and K, ZFe, KFe and KFe + Z (PM) catalysts were evaluated, as listed in Table S2.† The catalytic performance of the ZFe or KFe + Z (PM) catalyst alone is inferior to that of the KZFe catalyst. The presence of K promotes the formation of long-chain hydrocarbons. Apparently, the presence of K and Zn formed by spinel structure play a crucial role in improving the CO_2 hydrogenation performance, *e.g.*, improved adsorption and carburization ability, which is consistent with previous reports. The results also indicate that spinel KZFe is a promising catalyst for efficiently catalyzing the hydrogenation of CO_2 to long-chain hydrocarbons. Co-based catalysts have strong chain growth capacity and are generally used to produce long-chain hydrocarbons during traditional FTS. In view of this, a small amount of cobalt metal species was introduced into the iron-based catalyst system (KZFe–2.5Co), and it is found that the catalytic activity is improved while the selectivity of the target C_{5+} products is further improved from 49.9% to 55.2%. With further increase of the Co content (KZFe–5.0Co), the long-chain hydrocarbon selectivity reaches 57.8%, while the CO_2 conversion is as high as 50.2%, and the CO selectivity is as low as 8.1%. As the Co content is further increased, the selectivity of C_{5+} hydrocarbons decrease despite a slight increase in catalytic activity (KZFe–10.0Co and KZFe–20.0Co). Meanwhile, the CH_4 selectivity gradually increases. When the catalyst contains only Co metal, the product is mainly CH_4, since the Co species usually results in methanation in CO_2 hydrogenation (Table S2†). For comparison, a physical mixture of Co and KZFe catalyst was prepared to obtain KZFe + 5.0Co (PM). The long-chain hydrocarbon selectivity from KZFe + 5.0Co was inferior to that of KZFe–5.0Co, indicating that the manner of the incorporation of Co plays a crucial role in the catalytic performance. However, for the reference KZFe–SiO_2, the catalytic performance including activity and C_{5+} selectivity is rather lower than that of the KZFe catalyst, demonstrating that inert SiO_2 is harmful to improving the CO_2 hydrogenation performance.

In recent years, many research teams have focused on CO_2 hydrogenation to produce long-chain hydrocarbons and have developed a series of catalysts, such as promoter-modified Fe-based catalysts (K–Fe, Fe–Mn–K, *etc.*), composite catalysts ($Na–Fe_3O_4$ + ZSM-5, In_2O_3 + ZSM-5, *etc.*), and alloy catalysts (CoFe, *etc.*).[6–8,14,23,33,34] However, poor balance among catalytic activity, CO selectivity and target product selectivity often limit the yield of the target product (C_{5+}). In this case, the directionally designed bimetallic or alloy catalyst ($ZnFe_2O_4$–5.0Co) can maintain high catalytic activity (50.2% CO_2 conversion) while having high C_{5+} selectivity (57.8%) and low CO selectivity (8.1%), thus presenting a high yield of C_{5+}, which is higher than that of previous catalysts (26.7% C_{5+} yield for KZFe–5.0Co, Fig. 1b). In addition, the CO_2 hydrogenation activity and C_{5+} selectivity remain stable for 60 h (Fig. S2†). This indicates that KZFe–5.0Co is a promising catalyst for efficiently catalyzing CO_2 into long-chain hydrocarbons with high yield.

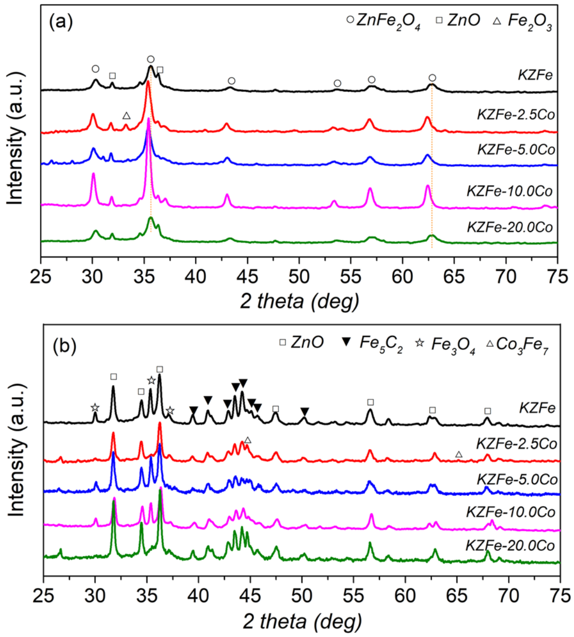

Fig. 2 (a) Powder XRD patterns of as-prepared KZFe, KZFe–2.5Co, KZFe–5.0Co, KZFe–10.0Co, and KZFe–20.0Co. (b) XRD patterns of the catalysts after CO_2 hydrogenation for 8 h.

The XRD patterns of the as-prepared and spent catalysts are shown in Fig. 2. For KZFe catalysts, the main phases are $ZnFe_2O_4$ (JCPDS, 77-0011) and ZnO (JCPDS, 89-0510) species. With the introduction of Co species, the characteristic diffraction peak of $ZnFe_2O_4$ moves towards the lower diffraction angle in XRD patterns, indicating that Co metal enters the system of $ZnFe_2O_4$ and forms $Zn(Fe_xCo_{2-x})O_4$. When the Co content is low, the presence of Fe_2O_3 (JCPDS, 89-8103) species can also be observed (KZFe–2.5Co). After reaction, for the KZFe catalyst, there exist three main phases, Fe_3O_4 (JCPDS, 89-3854), ZnO, and Fe_5C_2 (JCPDS, 20-0509) respectively.[35,36] However, for KZFe–2.5Co and KZFe–10.0Co, the peaks ascribed to Fe_3O_4 disappear, while the peaks corresponding to Co_3Fe_7 (JCPDS, 48-1817) appear. In contrast, the diffraction intensity of KZFe–5.0Co and KZFe–20.0Co is lower that of KZFe–2.5Co and KZFe–10.0Co, probably due to benign dispersion or the formation of small particles. However, no peaks corresponding to the CoFe alloy phase are observed for the KZFe + 5.0Co (PM) catalyst (Fig. S3†). For the hydrogenation of CO_2 to hydrocarbons, the first step is the RWGS reaction to form CO intermediates over Fe_3O_4, and then FTS occurs to form hydrocarbons over the surface of Fe_5C_2.[2] Yang *et al.* constructed Fe_5C_2/Co heterostructured nanoparticles to improve catalytic yield and suggested that Co with a lower energy barrier for CO dissociation can provide enough C1 building blocks while Fe_5C_2 is responsible for the chain growth.[37] Zhang *et al.* reported that a CoFe alloy is beneficial for the formation of jet fuels in CO_2 hydrogenation owing to the existence of metallic CoFe alloy phases.[14] It can be inferred that iron-based catalysts with different cobalt contents show great differences (Fig. 1 and Table S2†). Obviously, the presence of Co, which interacts with Fe, can efficiently tune the CO_2 hydrogenation performance. Additionally, the N_2 adsorption–desorption isotherms of different catalysts indicate that Co can affect the specific surface area (SSA) without a specific trend (Fig. S4 and Table S3†).

TEM was employed to characterize the spent catalysts (Fig. 3 and S5–S8†). For the KZFe catalyst, the lattice spacings of 0.296 nm and 0.265 nm can be attributed to the (220) plane of Fe_3O_4 and the (−311) plane of Fe_5C_2, respectively (Fig. S5†), which matches XRD pattern results well. With the introduction of Co (KZFe–2.5Co), a lattice spacing of 0.202 nm ascribed to the (110) plane of Co_3Fe_7 alloy can be observed (Fig. S6†). Similarly, specific lattice spacings corresponding to the (310) plane of Fe_3O_4, (−311) plane of Fe_5C_2, and (220) plane of Co_3Fe_7 phases are also observed for KZFe–5.0Co (Fig. 3a and b). Additionally, EDS line scanning profiles were used to investigate the distributions of different elements (Fig. 3c and d). It can be found that the Co species are highly adjacent to the Fe species (Fig. 3d). The line scanning at different positions also indicates

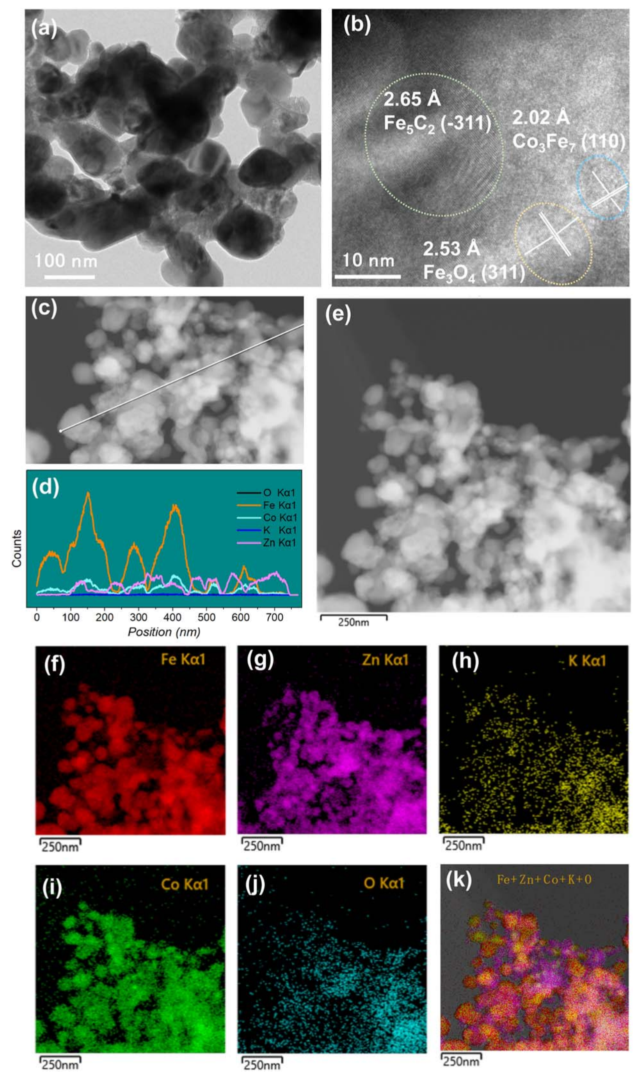

Fig. 3 (a and b) TEM and HR-TEM images, (c and d) line scanning, and (e–k) TEM image and corresponding EDS elemental maps of the spent KZFe–5.0Co catalyst after reaction.

the same phenomenon (Fig. S9†). To some extent, the overlapping of the Fe and Co signals further indicates the alloying of the elements Fe and Co. EDS elemental mapping depicts the uniform spatial surface distributions of the elements K, Fe, Zn, Co, and O (Fig. 3g–l). These results indicate that Fe and Co can effectively contact each other for catalyzing CO_2 hydrogenation (Fig. 3b, S6 and S8†). It is worth noting that although the specific surface area of KZFe–5.0Co is lower than that of KZFe–2.5Co and KZFe–10.0Co, the active phases can still disperse evenly, indicating that the specific surface area is not the key factor; instead, the formation of the active phase is the key factor. The introduction of a moderate amount of Co can reduce the formation of other non-ideal species while forming a sufficient amount of Co_3Fe_7 species.

EXAFS experiments were also conducted to study the fine structure of the spent catalysts (Fig. 4). Data reduction, data analysis, and EXAFS fitting were performed according to the standard procedures using the ATHENA and ARTEMIS program integrated within the Demeter packages.[38] The energy calibration of the sample was conducted using a standard Fe foil, which was simultaneously measured as a reference. For EXAFS modeling, the k^3-weighted EXAFS spectra were obtained *via* subtracting the post-edge background from the overall absorption, normalization with respect to the edge-jump step, and Fourier transformation to real (R) space using Hanning windows ($dk = 1.0$ Å) ranging from 3.0–11.0 $Å^{-1}$. The EXAFS of the Fe foil was fitted, and the value of the obtained amplitude reduction factor S_0^2 (0.762) was set in the EXAFS analysis to determine the coordination numbers (CNs) in the Fe–O/Fe/Co scattering path in the sample. With the incorporation of Co, the Fe K-edge for KZFe–5.0Co shifts to slightly lower energy and the white line concomitantly increases, which clearly reflects strong interaction between Fe and Co. The Fe–Fe(Co) and Fe–O coordination shells are observed, which indicates that the Fe_3O_4 active phases and Co_3Fe_7 alloy structure are formed (Fig. S10†). Fitting of the Fe K-edge EXAFS data also reveals these results (Table S4†).

H_2-TPR experiments were performed to compare the reducibilities of KZFe and Co-modified KZFe (Fig. S11†). For the KZFe catalyst, the overlapping peak can be divided into three stages, $ZnFe_2O_4$ to Fe_3O_4, Fe_3O_4 to FeO, and FeO to Fe. As shown, with the introduction of small Co species, the reduction temperature shifts towards low temperature (KZFe–2.5Co). The reduction temperature is further reduced with increasing Co content (KZFe–5.0Co). However, the reduction temperature changes slightly with further increasing the Co content (KZFe–10.0Co and KZFe–20.0Co). Apparently, the presence of Co is conducive to the reduction of iron oxide species to metallic Fe, which is consistent with previous reports.[16] The formed Fe will be converted into active iron species under the reaction conditions. Thus, improved reduction ability is beneficial for subsequent active phase formation. The adsorption of raw CO_2 molecules was investigated using CO_2-TPD experiments (Fig. S12†). Compared to the KZFe catalyst, the adsorption intensity of CO_2 increases over KZFe–2.5Co. With the further increase of Co, the adsorption intensity of CO_2 increases evidently, and new peaks at 241 °C and 323 °C appear (KZFe–5.0Co). A similar phenomenon can be also observed for KZFe–10.0Co and KZFe–20.0Co. This illustrates that the existence of Co can not only enhance the adsorption of acidic CO_2 molecules but also effectively strengthen the interaction between metal and CO_2 molecules, which is beneficial for the C1 species formation and chain propagation under real reaction conditions. Notably, for the inert SiO_2-supported KZFe catalyst, the reducing capacity of iron species is significantly reduced, which indicates that there is a strong interaction between metal species and the support (Fig. S13†). Additionally, with the utilization of SiO_2, the adsorption capacity of CO_x species was also reduced at the reaction temperature (Fig. S13†). These results indicate that the strong interaction between metal species and the inert SiO_2 support hinders the formation of active species and the adsorption of reaction molecules.

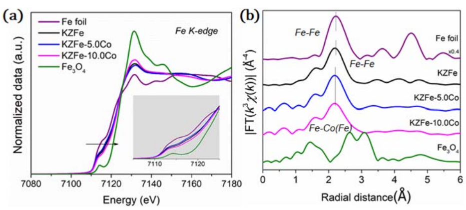

Fig. 4 (a) XANES spectrum of the Fe K-edge for different spent catalysts. (b) Fourier transformed EXAFS data for spent catalysts.

XPS was applied to investigate the phase composition and content of surface species (Fig. S14 and Table S5†). The binding energy peaks at 708.5, 710.9, and 712.0 eV in the Fe 2p spectrum are ascribed to Fe–C, Fe(II), and Fe(III).[39] For the SiO_2-supported KZFe catalysts, the main component is Fe(III), which also indicates that the strong metal–support interactions are not conducive to iron species reduction and active phase formation, which is accordance with the previous discussion (Table S5 and Fig. S13†). Inert SiO_2, which can form strong interactions with metal species, is not conducive to the formation of heavy hydrocarbons (Fig. 1). However, with the introduction of Co, the surface phase composition changes significantly. The Fe $2p_{1/2}$ peak intensity of Fe(III) decreases significantly, while those of Fe–C and Fe(II) increase significantly. Additionally, the binding energy position of the Fe(II) bond shifts toward low binding energy with the incorporation of Co, indicating the formation of electron-rich iron species (Fig. S14†). It has also been reported that increased electron density of the iron species during reaction can strengthen the Fe–C bond and weaken the C–O bond.[16,40] As summarized in Table S5,† it can be inferred that the introduction of Co can promote the transformation of Fe(III) into Fe(II) and Fe–C, which is essential to improve the CO_2 hydrogenation performance. The Co $2p_{3/2}$ spectra of the different spent catalysts were also compared (Fig. S15†). The introduction of a small amount of Co results in a higher Co^{2+} content (Table S6†). In part, this suggests that small amounts of Co are more likely to form alloying species. Additionally, the characteristic C 1s spectra of the spent catalysts can be deconvoluted into C–C/C=C at 298.5 eV, C–OH at 296.6 eV, C=O at 298.9, and O–C=OH at 299.7 eV.[41–43] As can be seen from the spectra, the surface of the KZFe catalyst is mainly composed of C–C/C═C and C–OH species. For all catalysts, C–C/C═C species are the dominant surface species, which is consistent with the CO_2 hydrogenation results (Fig. 1a). However, with the introduction of Co, more surface C═O and O–C═OH species appear (Fig. S16†). Interestingly, the peak intensity assigned to C–OH species from the Co-modified ones is rather lower than that of the KZFe catalyst. It is easy to infer that the presence of Co regulates the surface species of iron-based catalysts, producing more C═O and O–C═OH species. In addition, the surface analysis from the O 1s spectra also demonstrates similar results (Fig. S17†). The peaks at 298.3 eV, 230.1 eV, 531.4 eV, and 532.8 eV can be assigned to Co–O, Fe–O, Fe–OH, and H_2O (ad), respectively.[41,44–46] In addition, as a structure-sensitive reaction, the particle size has a significant impact on the reaction, especially the small-size particles (6–20 nm).[47,48] Based on TEM and refinement of XRD data, it can be found that the particle size is between 60 and 100 nm (Fig. 3 and S5–S8†), and the influence of these particle sizes on the CO_2 hydrogenation can be ignored. Additionally, refinement of XRD also showed that with the introduction of Co, the carbide content increased from 48.3 wt% to 50.2 wt% and the Co_3Fe_7 content was about 1.7 wt% (Fig. S18†).

To further clarify the promotional effect of Co and adsorbed reaction intermediates in CO_2 hydrogenation, *in situ* DRIFT spectra were recorded for the KZFe and KZFe–5.0Co catalysts during CO_2 hydrogenation (Fig. 5). Prior to reaction, the as-prepared catalysts were reduced at 400 °C under 5 vol% H_2 in Ar (50 mL min^{-1}) for 2 h. The *in situ* DRIFT spectra were collected from 1 min to 60 min at 1.0 MPa, 320 °C, and 20 mL min^{-1} of a gas mixture (24 vol% CO_2/70 vol% H_2/6 vol% Ar).

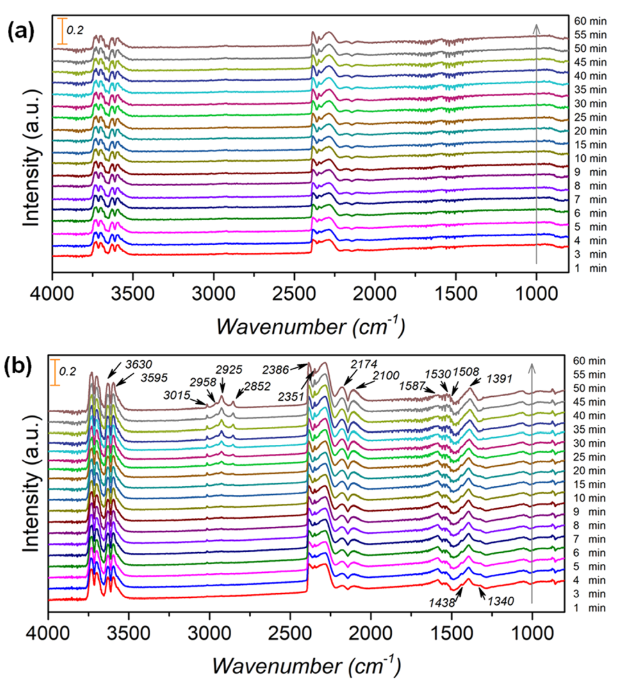

Fig. 5 *In situ* DRIFT spectra obtained during CO_2 hydrogenation over (a) KZFe and (b) KZFe–5.0Co (1.0 MPa, 320 °C, 20 mL min^{-1}).

For the KZFe catalyst, the bands at 2386 and 2351 cm^{-1} are assigned to gas-phase CO_2, and the bands appearing at 2174 and 2100 cm^{-1} are assigned to adsorption-state CO or gas-phase CO.[49] Additionally, bands ascribed to H_2O species can be observed at 3630 and 3595 cm^{-1}.[49] Apparently, the RWGS reaction occurs over KZFe and KZFe–5.0Co to form CO intermediates. In contrast, the adsorbed intermediates over the surface of KZFe–5.0Co are more complex than those over KZFe. For KZFe–5.0Co, the intensity corresponding to CO species increases as the reaction proceeds, indicating that Co promotes the RWGS reaction. Additionally, distinct peaks ascribed to intermediates are observed in the 1600–1200 cm^{-1} region. The bands at 1587 and 1391 cm^{-1}, 1508 and 1340 cm^{-1}, and 1438 cm^{-1} are assigned to the OCO vibration of formate (HCOO*), the asymmetric and symmetric vibrations of the monodentate carbonate (CO_3^{2}*), and the OH vibration of bicarbonate (HCO_3^*) or ionic carbonate (CO_3^{2}*), respectively.[50–52] This indicates that the presence of Co will promote surface O-containing species formation. Additionally, evident characteristic peaks in the region of 2900–3100 cm^{-1} appear. The bands at 2925 and 2852 cm^{-1} both correspond to the CH vibrations of CH_2 .[50] Compared to KZFe, Co incorporation into KZFe (KZFe–5.0Co) efficiently promotes the formation of more surface active hydrocarbons, and these species will be further converted into long-chain hydrocarbons.

For CO_2 hydrogenation, it is widely accepted that the CO formed from Fe_3O_4 generates hydrocarbons *via* a typical FTS process. For KZFe, the formed CO product can produce active CH_2^* fragments, which will then be converted into hydrocarbons *via* the carbide mechanism (Fig. 6a and c). However, with the incorporation of Co, oxygen-bearing intermediate species appeared (Fig. 5). The XPS results also indicate that more O–C═H and O═C species were produced over KZFe–5.0Co than KZFe (Fig. S16†). Except for Co_3Fe_7, the KZFe and KZFe–5.0Co catalysts have similar active phase types (Fig. 2, 3 and S5–S8†). However, the surface species on the two catalysts differed markedly (Fig. 5 and S16†), suggesting that the difference is due to the Co_3Fe_7 structure. It is therefore reasonable to assume that the O-containing species come from the surface of Co_3Fe_7 structure. As a consequence, a reaction scheme over the KZFe–5.0Co catalysts is proposed based on the above characterization and reaction results (Fig. 6c and d). For KZFe–5.0Co, Co and Fe form alloy species (Co_3Fe_7, Fig. 2–4) during the reaction. Correspondingly, the improved CO_2 adsorption behavior and the existence of bimetallic sites promote the formation of O-containing species (CO*, HCOO*, CO_3^{2}*, and HCO_3^*). Unlike in the carbide mechanism over the KZFe catalyst, these abundant oxygen-bearing intermediate species can further support the chain propagation reaction continuously *via* an oxygenate mechanism, and thus present high heavy hydrocarbon selectivity (Fig. 6b–d). For example, the HCOO* species undergo hydrogenation and C–O scission leading to CH_3O groups, and chain growth occurs by CO insertion into those R–O groups.[53] The HCOO* species could come from either the direct hydrogenation of adsorbed CO_2 or the interaction of CO intermediates and surface hydroxyl groups. In addition, CO* intermediates formed over Fe_3O_4 sites also undergo chain

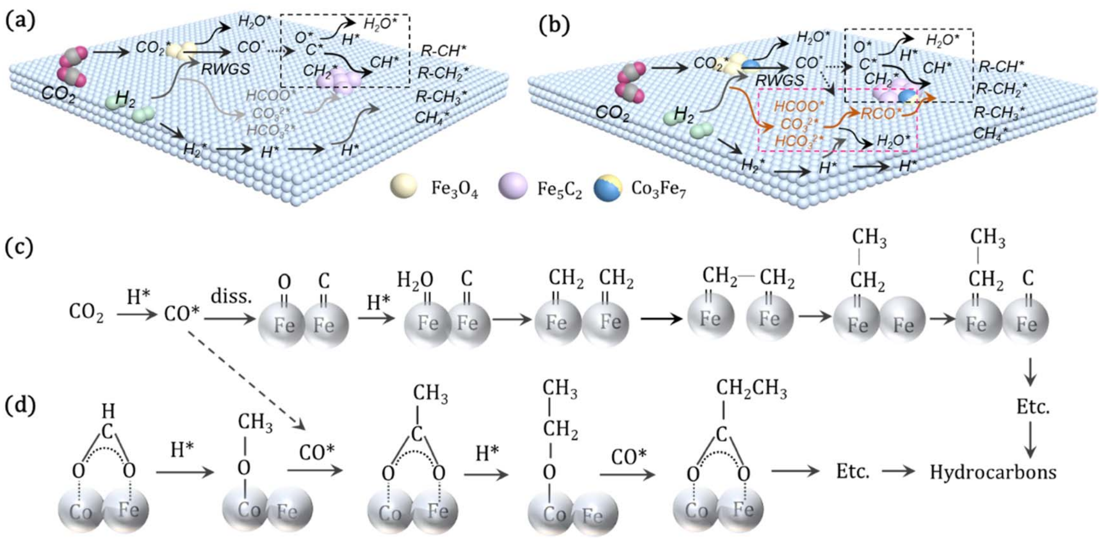

Fig. 6 Reaction scheme over the (a) KZFe and (b) KZFe–5.0Co catalysts for the directional synthesis of long-chain hydrocarbons from CO_2 hydrogenation. (c) Reaction path for long-chain hydrocarbon formation *via* the carbide mechanism, represented by black boxes in (a and b). (d) Oxygenate mechanism path for long-chain hydrocarbon formation, represented by the pink box in (b).

propagation *via* a carbide mechanism, and the active CO* is also involved in an oxygenation mechanism. The conversion of these surface species to long-chain hydrocarbons further drives the conversion of feedstock CO_2 molecules into these C1 species. Thus, the KZFe–5.0Co catalyst shows a high catalytic activity and low CO selectivity (Fig. 1). Furthermore, the harmful competition between the methanation reaction and O-containing species formation reaction will hinder the production of long-chain products with the excess addition of Co.

Conclusions

In summary, a series of Fe-based catalysts with Co modification were prepared by the sacrificial template method for the efficient conversion of CO_2 into long-chain hydrocarbons. The incorporation of Co improved the reduction and raw CO_2 molecule adsorption properties, thus facilitating metallic Fe formation and the carburization of Fe to generate active Fe_3O_4 and Fe_5C_2 phases. Additionally, Co has much a lower energy barrier for CO dissociation and can provide enough active C1 species (CO*, HCOO*, $CO_3{}^{2}*$, and HCO_3^*). Subsequently, the adsorbed C1 species undergo chain propagation *via* the oxygenate mechanism and carbide mechanism over the bimetallic sites and carbide sites, achieving high C_{5+} selectivity. The driving force from the bimetallic FeCo alloy sites is beneficial for enhancing CO_2 hydrogenation activity and decreasing CO selectivity in turn. Therefore, the tailor-made KZFe–5.0Co catalyst exhibits high activity (50.2%), low CO selectivity (8.1%), and high C_{5+} selectivity (57.8%), thus achieving a 26.7% yield of C_{5+}. The designed bimetallic catalyst sheds light on the highly efficient conversion of CO_2 to valuable hydrocarbons for practical industrial application, and provides new insights for the rational design of bimetallic or alloy catalysts.

Data availability

Data are available from the corresponding author upon reasonable request.

Author contributions

L. G. conducted all experiments and characterized the catalysts. L. G., S. S. and J. S. designed the experiments. L. G., S. S., J. S., and N. T. wrote the manuscript. L. G., Y. W., and S. S. were responsible for funding application. G. G., H. W., X. W. Y. K., and X. G. contributed to the analysis and interpretation of the data.

Conflicts of interest

There are no conflicts to declare.

Acknowledgements

The National Natural Science Foundation of China (U1832165, 21902001, 22102001), Key Research and Development Program of Anhui Province (202004a05020015, 006233172019), National Key Research and Development Program of China (2022YFA1604101), and DICP (Grant: DICP I202012) are greatly appreciated.

Notes and references

1 C. Hepburn, E. Adlen, J. Beddington, E. A. Carte, S. Fuss, N. M. Dowell, J. C. Minx, P. Smith and C. K. Williams, The technological and economic prospects for CO_2 utilization and removal, *Nature*, 2019, **575**, 87.

2 J. Wei, R. Yao, Y. Han, Q. Ge and J. Sun, Towards the development of the emerging process of CO_2 heterogenous hydrogenation into high-value unsaturated heavy hydrocarbons, *Chem. Soc. Rev.*, 2021, **50**, 10764–10805.

3 H. Li, C. Qiu, S. Ren, Q. Dong, S. Zhang, F. Zhou, X. Liang, J. Wang, S. Li and M. Yu, Na+-gated water-conducting nanochannels for boosting CO_2 conversion to liquid fuels, *Science*, 2020, **367**, 667–671.

4 H. Wang, Q. Lei, P. Li, C. Liu, Y. Xue, X. Zhang, C. Li and Z. Yang, Key CO_2 capture technology of pure oxygen exhaust gas combustion for syngas-fueled high-temperature fuel cells, *Int. J. Coal Sci. Technol.*, 2021, **8**(3), 383–393.

5 Q. Li, The view of technological innovation in coal industry under the vision of carbon neutralization, *Int. J. Coal Sci. Technol.*, 2021, **8**(6), 1197–1207.

6 B. Yao, T. Xiao, O. A. Makgae, X. Jie, S. Gonzalez-Cortes, S. Guan, A. I. Kirkland, J. R. Dilworth, H. A. Al-Megren, S. M. Alshihri, P. J. Dobson, G. P. Owen, J. M. Thomas and P. P. Edwards, Transforming carbon dioxide into jet fuel using an organic combustion-synthesized Fe-Mn-K catalyst, *Nat. Commun.*, 2020, **11**(1), 6395.

7 J. Wei, Q. Ge, R. Yao, Z. Wen, C. Fang, L. Guo, H. Xu and J. Sun, Directly converting CO_2 into a gasoline fuel, *Nat. Commun.*, 2017, **8**, 15174–15181.

8 P. Gao, S. Li, X. Bu, S. Dang, Z. Liu, H. Wang, L. Zhong, M. Qiu, C. Yang, J. Cai, W. Wei and Y. Sun, Direct conversion of CO_2 into liquid fuels with high selectivity over a bifunctional catalyst, *Nat. Chem.*, 2017, **9**, 1019–1024.

9 X. Ye, C. Yang, X. Pan, J. Ma, Y. Zhang, Y. Ren, X. Liu, L. Li and Y. Huang, Highly Selective Hydrogenation of CO_2 to Ethanol *via* Designed Bifunctional Ir_1-In_2O_3 Single-Atom Catalyst, *J. Am. Chem. Soc.*, 2020, **142**(45), 19001–19005.

10 Y. Ni, Z. Chen, Y. Fu, Y. Liu, W. Zhu and Z. Liu, Selective Conversion of CO_2 and H_2 into Aromatics, *Nat. Commun.*, 2018, **9**, 3457.

11 W. Zhou, K. Cheng, J. Kang, C. Zhou, V. Subramanian, Q. Zhang and Y. Wang, New horizon in C1 chemistry: breaking the selectivity limitation in transformation of syngas and hydrogenation of CO_2 into hydrocarbon chemicals and fuels, *Chem. Soc. Rev.*, 2019, **48**, 3193–3228.

12 R.-P. Ye, J. Ding, W. Gong, M. D. Argyle, Q. Zhong, Y. Wang, C. K. Russell, Z. Xu, A. G. Russell, Q. Li, M. Fan and Y.-G. Yao, CO_2 hydrogenation to high-value products *via* heterogeneous catalysis, *Nat. Commun.*, 2019, **10**, 5698.

13 S. Wang, T. Wu, J. Lin, Y. Ji, S. Yan, Y. Pei, S. Xie, B. Zong and M. Qiao, Iron–Potassium on Single-Walled Carbon Nanotubes as Efficient Catalyst for CO_2 Hydrogenation to Heavy Olefins, *ACS Catal.*, 2020, **10**(11), 6389–6401.

14 L. Zhang, Y. Dang, X. Zhou, P. Gao, A. Petrus van Bavel, H. Wang, S. Li, L. Shi, Y. Yang, E. I. Vovk, Y. Gao and Y. Sun, Direct conversion of CO_2 to a jet fuel over CoFe alloy catalysts, *The Innovation*, 2021, **2**(4), 100170.

15 Q. Xu, X. Xu, G. Fan, L. Yang and F. Li, Unveiling the roles of Fe-Co interactions over ternary spinel-type $ZnCo_xFe_{2-x}O_4$ catalysts for highly efficient CO_2 hydrogenation to produce light olefins, *J. Catal.*, 2021, **400**, 355–366.

16 L. Guo, J. Li, Y. Cui, R. Kosol, Y. Zeng, G. Liu, J. Wu, T. Zhao, G. Yang, L. Shao, P. Zhan, J. Chen and N. Tsubaki, Spinel-structure catalyst catalyzing CO_2 hydrogenation to full spectrum alkenes with an ultra-high yield, *Chem. Commun.*, 2020, **56**, 9372–9375.

17 X. Nie, H. Wang, M. J. Janik, Y. Chen, X. Guo and C. Song, Mechanistic Insight into C–C Coupling over Fe–Cu Bimetallic Catalysts in CO_2 Hydrogenation, *J. Phys. Chem. C*, 2017, **121**(24), 13164–13174.

18 L. Wang, L. Wang, J. Zhang, X. Liu, H. Wang, W. Zhang, Q. Yang, J. Ma, X. Dong, S. J. Yoo, J.-G. Kim, X. Meng and F.-S. Xiao, Selective Hydrogenation of CO_2 to Ethanol over Cobalt Catalysts, *Angew. Chem., Int. Ed.*, 2018, **130**, 1–6.

19 K. Y. Kim, H. Lee, W. Y. Noh, J. Shin, S. J. Han, S. K. Kim, K. An and J. S. Lee, Cobalt Ferrite Nanoparticles to Form a Catalytic Co–Fe Alloy Carbide Phase for Selective CO_2 Hydrogenation to Light Olefins, *ACS Catal.*, 2020, **10**(15), 8660–8671.

20 M. Fujiwara, R. Kieffer, H. Ando and Y. Souma, Development of composite catalysts made of Cu-Zn-Cr oxide/zeolite for the hydrogenation of carbon dioxide, *Appl. Catal., A*, 1995, **121**, 113–124.

21 X. Wang, G. Yang, J. Zhang, S. Chen, Y. Wu, Q. Zhang, J. Wang, Y. Han and Y. Tan, Synthesis of isoalkanes over a core (Fe-Zn-Zr)- shell (zeolite) catalyst by CO_2 hydrogenation, *Chem. Commun.*, 2016, **52**, 7352–7355.

22 Z. Shi, H. Yang, P. Gao, X. Chen, H. Liu, L. Zhong, H. Wang, W. Wei and Y. Sun, Effect of alkali metals on the performance of $CoCu/TiO_2$ catalysts for CO_2 hydrogenation to long-chain hydrocarbons, *Chin. J. Catal.*, 2018, **39**(8), 1294–1302.

23 Y. H. Choi, Y. J. Jang, H. Park, W. Y. Kim, Y. H. Lee, S. H. Choi and J. S. Lee, Carbon dioxide Fischer-Tropsch synthesis: A new path to carbon-neutral fuels, *Appl. Catal., B*, 2017, **202**, 605–610.

24 N. Boreriboon, X. Jiang, C. Song and P. Prasassarakich, Fe-based bimetallic catalysts supported on TiO_2 for selective CO_2 hydrogenation to hydrocarbons, *J. CO2 Util.*, 2018, **25**, 330–337.

25 J. Wei, J. Sun, Z. Wen, C. Fang, Q. Ge and H. Xu, New insights into the effect of sodium on Fe_3O_4-based nanocatalysts for CO_2 hydrogenation to light olefins, *Catal. Sci. Technol.*, 2016, **6**(13), 4786–4793.

26 M. Albrecht, U. Rodemerck, M. Schneider, M. Bröring, D. Baabe and E. V. Kondratenko, Unexpectedly efficient CO_2 hydrogenation to higher hydrocarbons over non-doped Fe_2O_3, *Appl. Catal., B*, 2017, **204**, 119–126.

27 Y. Wang, L. Tan, M. H. Tan, P. P. Zhang, Y. Fang, Y. Yoneyama, G. H. Yang and N. Tsubaki, Rationally Designing Bifunctional Catalysts as an Efficient Strategy to Boost CO_2 Hydrogenation Producing Value-Added Aromatics, *ACS Catal.*, 2019, **9**, 895–901.

28 Y. H. Choi, E. C. Ra, E. H. Kim, K. Y. Kim, Y. J. Jang, K.-N. Kang, S. H. Choi, J.-H. Jang and J. S. Lee, Sodium-Containing Spinel Zinc Ferrite as a Catalyst Precursor for the Selective Synthesis of Liquid Hydrocarbon Fuels, *ChemSusChem*, 2017, **10**, 4764–4770.

29 T. Numpilai, T. Witoon, N. Chanlek, W. Limphirat, G. Bonura, M. Chareonpanich and J. Limtrakul, Structure–activity relationships of Fe-Co/K-Al_2O_3 catalysts calcined at different temperatures for CO_2 hydrogenation to light olefins, *Appl. Catal., A*, 2017, **547**, 219–229.

30 L. Guo, S. Sun, J. Li, W. Gao, H. Zhao, B. Zhang, Y. He, P. Zhang, G. Yang and N. Tsubaki, Boosting liquid hydrocarbons selectivity from CO_2 hydrogenation by facilely tailoring surface acid properties of zeolite *via* a modified Fischer-Tropsch synthesis, *Fuel*, 2021, **306**, 121684.

31 F. Jiang, B. Liu, S. Geng, Y. Xu and X. Liu, Hydrogenation of CO_2 into hydrocarbons: enhanced catalytic activity over Fe-based Fischer–Tropsch catalysts, *Catal. Sci. Technol.*, 2018, **8**(16), 4097–4107.

32 A. Noreen, M. Li, Y. Fu, C. C. Amoo, J. Wang, E. Maturura, C. Du, R. Yang, C. Xing and J. Sun, One-Pass Hydrogenation of CO_2 to Multibranched Isoparaffins over Bifunctional Zeolite-Based Catalysts, *ACS Catal.*, 2020, **10**(23), 14186–14194.

33 W. D. Shafer, G. Jacobs, U. M. Graham, H. H. Hamdeh and B. H. Davis, Increased CO_2 Hydrogenation to Liquid Products Using Promoted Iron Catalysts, *J. Catal.*, 2019, **369**, 239–248.

34 Y. Wang, G. Wang, L. I. v. d. Wal, K. Cheng, Q. Zhang, K. P. d. Jong and Y. Wang, Visualizing Element Migration over Bifunctional Metal-Zeolite Catalysts and its Impact on Catalysis, *Angew. Chem., Int. Ed.*, 2021, **60**(32), 17735–17743.

35 Y. Xu, J. Wang, G. Ma, J. Bai, Y. Du and M. Ding, Selective conversion of syngas to olefins-rich liquid fuels over core-shell FeMn@SiO_2 catalysts, *Fuel*, 2020, **275**, 117884.

36 J. Zhu, P. Wang, X. Zhang, G. Zhang, R. Li, W. Li, T. P. Senftle, W. Liu, J. Wang, Y. Wang, A. Zhang, Q. Fu, C. Song and X. Guo, Dynamic structural evolution of iron catalysts involving competitive oxidation and carburization during CO_2 hydrogenation, *Sci. Adv.*, 2022, (8), eabm3629.

37 C. Yang, B. Zhao, R. Gao, S. Yao, P. Zhai, S. Li, J. Yu, Y. Hou and D. Ma, Construction of Synergistic Fe_5C_2/Co Heterostructured Nanoparticles as an Enhanced Low Temperature Fischer-Tropsch Synthesis Catalyst, *ACS Catal.*, 2017, **7**, 5661–5667.

38 B. Ravel and M. Newville, ATHENA, ARTEMIS, HEPHAESTUS: data analysis for X-ray absorption spectroscopy using IFEFFIT, *J. Synchrotron Radiat.*, 2005, **12**(Pt 4), 537–541.

39 L. Guo, J. Sun, X. Ji, J. Wei, Z. Wen, R. Yao, H. Xu and Q. Ge, Directly converting carbon dioxide to linear α-olefins on bio-promoted catalysts, *Commun. Chem.*, 2018, **1**, 11.

40 J. Lu, L. Yang, B. Xu, Q. Wu, D. Zhang, S. Yuan, Y. Zhai, X. Wang, Y. Fan and Z. Hu, Promotion Effects of Nitrogen Doping into Carbon Nanotubes on Supported Iron Fischer–Tropsch Catalysts for Lower Olefins, *ACS Catal.*, 2014, **4**(2), 613–621.

41 J. M. Cho, B.-G. Kim, G. Y. Han, J. Sun, H.-K. Jeong and J. W. Bae, Effects of metal-organic framework-derived iron carbide phases for CO hydrogenation activity to hydrocarbons, *Fuel*, 2020, **281**, 118779.

42 M. Fan, C. Zhu, Z.-Q. Feng, J. Yang, L. Liu and D. Sun, Preparation of N-doped graphene by reduction of graphene oxide with mixed microbial system and its haemocompatibility, *Nanoscale*, 2014, **6**(9), 4882–4888.

43 Y. Zhao, J. Zhang, X. Guo, H. Fan, W. Wu, H. Liu and G. Wang, Fe_3C@nitrogen doped CNT arrays aligned on nitrogen functionalized carbon nanofibers as highly efficient catalysts for the oxygen evolution reaction, *J. Mater. Chem. A*, 2017, **5**(37), 19672–19679.

44 A. F. Lucrédio, G. T. Filho and E. M. Assaf, Co/Mg/Al hydrotalcite-type precursor, promoted with La and Ce, studied by XPS and applied to methane steam reforming reactions, *Appl. Surf. Sci.*, 2009, **255**(11), 5851–5856.

45 P. Chen, T. Zhou, S. Wang, N. Zhang, Y. Tong, H. Ju, W. Chu, C. Wu and Y. Xie, Dynamic Migration of Surface Fluorine Anions on Cobalt-Based Materials to Achieve Enhanced Oxygen Evolution Catalysis, *Angew. Chem., Int. Ed.*, 2018, **57**(47), 15471–15475.

46 L. Cao, W. Liu, Q. Luo, R. Yin, B. Wang, J. Weissenrieder, M. Soldemo, H. Yan, Y. Lin, Z. Sun, C. Ma, W. Zhang, S. Chen, H. Wang, Q. Guan, T. Yao, S. Wei, J. Yang and J. Lu, Atomically dispersed iron hydroxide anchored on Pt for preferential oxidation of CO in H_2, *Nature*, 2019, **565**(7741), 631–635.

47 H. M. T. Galvis, J. H. Bitter, T. Davidian, M. Ruitenbeek, A. I. Dugulan and K. P. d. Jong, Iron particle size effects for direct production of lower olefins from synthesis gas, *J. Am. Chem. Soc.*, 2012, **134**(39), 16207–16215.

48 L. Guo, P. Zhang, Y. Cui, G. Liu, J. Wu, G. Yang, Y. Yoneyama and N. Tsubaki, One-Pot Hydrothermal Synthesis of Nitrogen Functionalized Carbonaceous Material Catalysts with Embedded Iron Nanoparticles for CO_2 Hydrogenation, *ACS Sustainable Chem. Eng.*, 2019, **7**, 8331–8339.

49 L. Guo, Y. Cui, H. Li, Y. Fang, R. Prasert, J. Wu, G. Yang, Y. Yoneyama and N. Tsubaki, Selective formation of linear-alpha olefins by catalyzing CO_2 hydrogenation over a bimetallic catalyst, *Catal. Commun.*, 2019, **130**, 105759.

50 J. Zhu, G. Zhang, W. Li, X. Zhang, F. Ding, C. Song and X. Guo, Deconvolution of the Particle Size Effect on CO_2 Hydrogenation over Iron-Based Catalysts, *ACS Catal.*, 2020, **10**(13), 7424–7433.

51 H. Jo, M. K. Khan, M. Irshad, M. W. Arshad, S. K. Kim and J. Kim, Unraveling the role of cobalt in the direct conversion of CO_2 to high-yield liquid fuels and lube base oil, *Appl. Catal., B*, 2022, **305**, 121041.

52 Q. Sheng, R.-P. Ye, W. Gong, X. Shi, B. Xu, M. Argyle, H. Adidharma and M. Fan, Mechanism and catalytic performance for direct dimethyl ether synthesis by CO_2 hydrogenation over CuZnZr/ferrierite hybrid catalyst, *J. Environ. Sci.*, 2020, **92**, 106–117.

53 A. Frennet, T. V. d. Bocarmé, J.-M. Bastin and N. Kruse, Mechanism and Kinetics of the Catalytic CO-H_2 Reaction: An Approach by Chemical Transients and Surface Relaxation Spectroscopy, *J. Phys. Chem. B*, 2005, **109**, 2350–2359.